

Thermodynamics of hexagonal-close-packed iron under Earth's core conditions

D. Alfè,^{1,2} G. D. Price,¹ and M. J. Gillan²

¹*Research School of Geological and Geophysical Sciences, Birkbeck and University College London, Gower Street, London WC1E 6BT, United Kingdom*

²*Physics and Astronomy Department, University College London, Gower Street, London WC1E 6BT, United Kingdom*
(Received 26 August 1999; revised manuscript received 7 December 2000; published 9 July 2001)

The free energy and other thermodynamic properties of hexagonal-close-packed iron are calculated by direct *ab initio* methods over a wide range of pressures and temperatures relevant to the Earth's core. The *ab initio* calculations are based on density-functional theory in the generalized-gradient approximation, and are performed using the projector augmented wave approach. Thermal excitation of electrons is fully included. The Helmholtz free energy consists of three parts, associated with the rigid perfect lattice, harmonic lattice vibrations, and anharmonic contributions, and the technical problems of calculating these parts to high precision are investigated. The harmonic part is obtained by computing the phonon frequencies over the entire Brillouin zone, and by summation of the free-energy contributions associated with the phonon modes. The anharmonic part is computed by the technique of thermodynamic integration using carefully designed reference systems. Detailed results are presented for the pressure, specific heat, bulk modulus, expansion coefficient and Grüneisen parameter, and comparisons are made with values obtained from diamond-anvil-cell and shock experiments.

DOI: 10.1103/PhysRevB.64.045123

PACS number(s): 71.15.-m, 64.10.+h, 62.50.+g

I. INTRODUCTION

Ab initio techniques based on density-functional theory (DFT) have played a key role for several years in the study of matter under extreme conditions.¹ With recent progress in the direct *ab initio* calculation of thermodynamic free energies,²⁻⁴ there is now great scope for the systematic and accurate calculation of thermodynamic properties over a wide range of conditions. We present here extensive DFT calculations of the free energy of hexagonal-close-packed (hcp) iron under Earth's core conditions, which we have used to obtain results for a number of other thermodynamic quantities, including the bulk modulus, expansion coefficient, specific heat and Grüneisen parameter. For some of these we can make direct comparisons with experimental data, which support the accuracy and realism of the calculations; for others, the calculations supply information that is not yet available from experiments. An important ambition of the work is to determine thermodynamic functions without making any significant statistical-mechanical or electronic-structure approximations, other than those required by DFT itself, and we shall argue that we come close to achieving this. The techniques we have developed are rather general, and we believe they will find application to many other problems concerning matter under extreme conditions.

The importance of understanding the high-pressure and high-temperature properties of iron can be appreciated by recalling that the Earth's core accounts for about 30% of the mass of the entire Earth, and consists mainly of iron.⁵ In fact, the liquid outer core is somewhat less dense than pure iron, and is generally accepted to contain light impurities such as S, O, Si or H;⁶ probably the density of the solid inner core is also significantly reduced by impurities.^{7,8} Nevertheless, the thermodynamic properties of pure iron are fundamental to understanding the more complex real material in the core,

and a large experimental effort has been devoted to measuring them. The difficulties are severe, because the pressure range of interest extends from 100 GPa up to nearly 400 GPa, and the temperature goes from ca. 3000 K to perhaps 7000 K—the temperature at the center of the core is subject to an uncertainty of at least 1000 K.

Static compression experiments with the diamond anvil cell (DAC) have been performed on Fe up to 300 GPa at room temperature,⁹ and DAC experiments at temperatures as high as 3700 K have been reported up to 200 GPa.¹⁰⁻¹⁸ Our present knowledge of the phase diagram of Fe comes mainly from these experiments, though there are still controversies. For pressures p above ca. 60 GPa and temperatures T below ca. 1500 K it is generally accepted that the stable phase is hexagonal close packed (hcp). Recent DAC diffraction experiments¹⁸ indicate that hcp is actually stable for all temperatures up to the melting line for $p > 60$ GPa, but earlier work claimed that there is another phase, usually called β , in a region below the melting line for pressures above ca. 40 GPa. The existing evidence suggests that, if the β -phase is thermodynamically stable, its structure could either be double-hcp,^{14,15} or orthorhombic,¹⁷ and in either case is closely related to the usual hcp structure. According to very recent theoretical work,¹⁹ hcp is thermodynamically slightly more stable than double-hcp at Earth's core pressures and temperatures. The evidence for the stability of hcp over much of the high-temperature/high-pressure phase diagram is our motivation for concentrating on this phase in the present work.

DAC measurements have given some information about thermodynamic quantities up to pressures of a few tens of GPa, but beyond this shock experiments (see, e.g., Refs. 20-22) have no competitors. These experiments give direct values of the pressure as a function of volume²¹ on the Hugoniot curve, and have also been used to obtain information about the adiabatic bulk modulus and some other thermody-

dynamic quantities on this curve. These data will be important in validating our calculations. Temperature is difficult to measure reliably in shock experiments,²² and we believe that our *ab initio* results may be valuable in providing the needed calibration.

The difficulties and uncertainties of experiments have stimulated many theoretical efforts. Some of the theoretical work has been based on simple atomistic models, such as a representation of the total energy as a sum of pair potentials,²³ or the more sophisticated embedded-atom model.²⁴ Such models can be useful, but for accuracy and reliability they cannot match high-quality *ab initio* calculations based on DFT.²⁵ The accuracy of DFT depends very much on the approximation used for the electronic exchange-correlation energy E_{xc} . It is known that the local density approximation (LDA) is not fully satisfactory for Fe,²⁶ but that modern generalized-gradient approximations (GGA) reproduce a wide range of properties very accurately. These include the equilibrium lattice parameter, bulk modulus and magnetic moment of body-centered cubic (bcc) Fe at ambient pressures,^{27–29} and the phonon dispersion relations of the bcc phase.^{19,32,69} There has been much DFT work on different crystal structures of Fe at high pressures, and experimental low-temperature results for the pressure as a function of volume $p(V)$ up to $p=300$ GPa for the hcp structure are accurately predicted.⁹ Further evidence for the accuracy of DFT comes from the successful prediction of the bcc to hcp transition pressure,^{27,28} and comparison with the measured phonon density of states of the hcp phase up to pressures of ~ 150 GPa.³⁰ With *ab initio* molecular dynamics, DFT calculations can also be performed on the liquid state, and we have reported extensive calculations both on pure liquid Fe^{29,31,32} and on liquid Fe/S and Fe/O alloys.^{33–35}

Recently, work has been reported^{8,36} in which the thermal properties of close-packed crystalline Fe under Earth's core conditions are calculated using *ab initio* methods. In fact, the work itself was based on a tight-binding representation of the total energy, but this was parametrized using extensive *ab initio* data. The authors did not attempt to perform the statistical-mechanical calculations exactly, but instead used the so-called ‘‘particle in a cell’’ approximation,³⁷ in which vibrational correlations between atoms are ignored. In spite of these limitations, the work yielded impressive agreement with shock data. We shall make comparisons with this work at various points in the present paper.

The present DFT work is based on the GGA known as Perdew-Wang 1991.^{38,39} The choice of functional for exchange-correlation energy E_{xc} exactly determines the free energy and all other thermodynamic quantities. By this, we simply mean that E_{xc} exactly determines the total energy of the system $U(\mathbf{R}_1, \dots, \mathbf{R}_N)$ as a function of atomic positions $\{\mathbf{R}_i\}$, and the standard formulas of statistical mechanics express the free energy F exactly in terms of $U(\mathbf{R}_1, \dots, \mathbf{R}_N)$. The calculation of U from E_{xc} has been discussed over many years by many authors. The present work is based on the projector-augmented-wave (PAW) implementation of DFT,^{32,40,41} which is an all-electron technique similar to other standard implementations such as full-potential linear augmented plane waves (FLAPW),⁴² as well as being closely

related to the ultrasoft pseudopotential (USPP) method.⁴⁶ In principle, PAW allows one to compute U with any required precision from a given E_{xc} . In practical tests on Fe and other systems,^{32,41} the technique has been shown to yield results that are almost indistinguishable from calculations based on FLAPW, USPP and other DFT implementations. We aim to demonstrate in this work that F can also be computed from the *ab initio* $U(\mathbf{R}_1, \dots, \mathbf{R}_N)$ to any required precision.

To clarify the precision we are aiming for in the calculation of F , we need to explain that one of the future objectives of this work is the *ab initio* determination of the high-pressure melting properties of Fe, a preliminary report on which has been published elsewhere⁴³ (see also Refs. 44 and 45). Our proposed strategy for determining the melting curve starts from the basic principle that at coexistence the Gibbs free energies $G_{\text{sol}}(p, T)$ and $G_{\text{liq}}(p, T)$ of solid and liquid are equal. But for a given pressure, the curves of $G_{\text{sol}}(p, T)$ and $G_{\text{liq}}(p, T)$ cross at a shallow angle. The difference of slopes $(\partial G_{\text{sol}}/\partial T)_p = -S_{\text{sol}}$ and $(\partial G_{\text{liq}}/\partial T)_p = -S_{\text{liq}}$ is equal to the entropy of fusion $S_m \equiv S_{\text{liq}} - S_{\text{sol}}$, which is comparable to k_B per atom. This means that to get the melting temperature within an error of δT , the noncancelling errors in G_{sol} and G_{liq} must not exceed ca. $k_B \delta T$. Ideally, we should like to calculate the melting temperature to within ca. 100 K, so that noncancelling errors must be reduced to the level of ca. 10 meV. Our original ambition for the present work on hcp Fe was to obtain F from the given *ab initio* $U(\mathbf{R}_1, \dots, \mathbf{R}_N)$ to this precision, and to demonstrate that this has been achieved. As we shall see, this target has probably not been attained, but we miss it by only a small factor, which will be estimated.

We shall present results for thermodynamic quantities for pressures $50 < p < 400$ GPa and temperatures $2000 < T < 6000$ K. This is a far wider range than is strictly needed for understanding the inner core, where pressures span the range $330 < p < 364$ GPa and T is believed to be in the region of $5000 - 6000$ K. However, the wider range is essential in making comparisons with the available laboratory data. We set the lower limit of 2000 K for our T range because this is the lowest T that has been proposed for equilibrium between the hcp crystal and the liquid (at lower T , melting occurs from the fcc phase).

In the next section, we summarize the *ab initio* techniques, and give a detailed explanation of the statistical-mechanical techniques. The three sections after that present our investigations of the three main components of the free energy, associated with the rigid perfect lattice, harmonic lattice vibrations, and anharmonic contributions, probing in each case the technical measures that must be taken to achieve our target precision. Section VI reports our results for all the thermodynamic quantities derived from the free energy, with comparisons wherever possible with experimental measurements and previous theoretical values. Overall discussion and conclusions are given in Sec. VII. The problem of choosing good reference models for the calculation of the anharmonic free energy is discussed in an Appendix. The implications of our results for deepening our understanding of the Earth's core will be analyzed elsewhere.

II. TECHNIQUES

A. *Ab initio* techniques

The use of DFT to calculate the energetics of many-atom systems has been extensively reviewed.²⁵ Thermal electronic excitations play a crucial role in the current work, and we handle these using the standard methods of finite-temperature DFT developed by Mermin.^{47–49} The fundamental quantity is the electronic free energy $U(\mathbf{R}_1, \dots, \mathbf{R}_N; T_{\text{el}})$ calculated at electronic temperature T_{el} with the N nuclei fixed at positions $\mathbf{R}_1, \dots, \mathbf{R}_N$. This is given by $U = E - TS$, where the DFT energy E is the usual sum of kinetic, electron-nucleus, Hartree, and exchange-correlation terms, and S is the electronic entropy, given by the independent-electron formula $S = -2k_{\text{B}}T_{\text{el}} \sum_i [f_i \ln f_i + (1-f_i) \ln(1-f_i)]$, with f_i the thermal (Fermi-Dirac) occupation number of orbital i . The electronic kinetic energy and other parts of E also contain the occupation numbers. In exact DFT, the exchange-correlation (free) energy E_{xc} has an explicit dependence on T_{el} . Very little is known about this dependence, and we assume here that E_{xc} has its zero-temperature form.

Throughout this work, we treat the statistical mechanics of the nuclei in the classical limit, and we show later that quantum corrections are negligible under the conditions of interest. The Helmholtz free energy of the whole system is then

$$F = -k_{\text{B}}T \ln \left\{ \frac{1}{N! \Lambda^{3N}} \int d\mathbf{R}_1 \dots d\mathbf{R}_N \times \exp[-\beta U(\mathbf{R}_1, \dots, \mathbf{R}_N; T_{\text{el}})] \right\}, \quad (1)$$

where $\Lambda = h/(2\pi M k_{\text{B}}T)^{1/2}$ is the thermal wavelength, with M the nuclear mass, and $\beta = 1/k_{\text{B}}T$. In practice, the electronic and nuclear degrees of freedom are in thermal equilibrium with each other, so that $T_{\text{el}} = T$, but it will be useful to keep the logical distinction between the two. Although $U(\mathbf{R}_1, \dots, \mathbf{R}_N)$ is really a *free* energy, we will generally call it the total energy function, to avoid confusion with the overall free energy F .

The PAW implementation of DFT has been described in detail in previous papers.^{40,41} The present calculations were done using the VASP code.^{50,51} The details of the core radii, augmentation-charge cutoffs, etc., are exactly as in our recent PAW work on liquid Fe.³² Our division into valence and core states is also the same: the $3p$ electrons are treated as core states, but their response to the high compression is represented by an effective pair potential, with the latter constructed using PAW calculations in which the $3p$ states are explicitly included as valence states. Further technical details are as follows. All the calculations are based on the form of GGA known as Perdew-Wang 1991.^{38,39} Brillouin-zone sampling was performed using Monkhorst-Pack special points,⁵² and the detailed form of sampling will be noted where appropriate. The plane-wave cutoff of 300 eV was used, exactly as in our PAW work on liquid Fe.

B. Components of the free energy

Our *ab initio* calculations of thermodynamic properties are based on a separation of the Helmholtz free energy F into the three components mentioned in the Introduction, which are associated with the rigid perfect crystal, harmonic lattice vibrations, and anharmonic contributions.

To explain this separation, we start from the expression for F given in Eq. (1). We let $F_{\text{perf}}(T_{\text{el}}) \equiv U(\mathbf{R}_1^0, \dots, \mathbf{R}_N^0; T_{\text{el}})$ denote the total free energy of the system when all atoms are fixed at their perfect-lattice positions \mathbf{R}_I^0 , and write $U(\mathbf{R}_1, \dots, \mathbf{R}_N; T_{\text{el}}) = F_{\text{perf}}(T_{\text{el}}) + U_{\text{vib}}(\mathbf{R}_1, \dots, \mathbf{R}_N; T_{\text{el}})$, which defines the vibrational energy U_{vib} . Then it follows from Eq. (1) that

$$F = F_{\text{perf}} + F_{\text{vib}}, \quad (2)$$

where the vibrational free energy F_{vib} is given by

$$F_{\text{vib}} = -k_{\text{B}}T \ln \left\{ \frac{1}{\Lambda^{3N}} \int d\mathbf{R}_1 \dots d\mathbf{R}_N \times \exp[-\beta U_{\text{vib}}(\mathbf{R}_1, \dots, \mathbf{R}_N; T_{\text{el}})] \right\}. \quad (3)$$

(Note that we now omit the factor $N!$ from the partition function, since every atom is assumed to be confined to its own lattice site.) The vibrational energy U_{vib} can be further separated into harmonic and anharmonic parts ($U_{\text{vib}} = U_{\text{harm}} + U_{\text{anharm}}$), in terms of which we can define the harmonic vibrational free energy F_{harm} :

$$F_{\text{harm}} = -k_{\text{B}}T \ln \left\{ \frac{1}{\Lambda^{3N}} \int d\mathbf{R}_1 \dots d\mathbf{R}_N \times \exp[-\beta U_{\text{harm}}(\mathbf{R}_1, \dots, \mathbf{R}_N; T_{\text{el}})] \right\}, \quad (4)$$

with the anharmonic free energy being the remainder $F_{\text{anharm}} = F_{\text{vib}} - F_{\text{harm}}$. The harmonic energy U_{harm} is defined in the obvious way:

$$U_{\text{harm}} = \frac{1}{2} \sum_{I,J} \mathbf{u}_I \cdot (\nabla_I \nabla_J U) \cdot \mathbf{u}_J, \quad (5)$$

where \mathbf{u}_I is the displacement of atom I from its perfect-lattice position ($\mathbf{u}_I \equiv \mathbf{R}_I - \mathbf{R}_I^0$) and the double gradient of the *ab initio* total energy is evaluated with all atoms at their perfect-lattice positions. Since we are dealing with a crystal, we shall usually prefer to rewrite U_{harm} in the more explicit form:

$$U_{\text{harm}} = \frac{1}{2} \sum_{ls\alpha, l't\beta} u_{ls\alpha} \Phi_{ls\alpha, l't\beta} u_{l't\beta}, \quad (6)$$

where $u_{ls\alpha}$ is the α th Cartesian component of the displacement of atom number s in primitive cell number l , and $\Phi_{ls\alpha, l't\beta}$ is the force-constant matrix. It should be noted that the present separation of F does not represent a separation into electronic and nuclear contributions, since thermal electronic excitations influence all three parts of F .

Since all other thermodynamic functions can be obtained by taking appropriate derivatives of the Helmholtz free energy, the separation of F into components implies a similar separation of other quantities. For example, the pressure $p = -(\partial F/\partial V)_T$ is $p_{\text{perf}} + p_{\text{harm}} + p_{\text{anharm}}$, where $p_{\text{perf}} = -(\partial F_{\text{perf}}/\partial V)_T$, and similarly for the components p_{harm} and p_{anharm} .

C. Phonon frequencies

The free energy of a harmonic oscillator of frequency ω is $k_B T \ln(\exp(\frac{1}{2}\beta\hbar\omega) - \exp(-\frac{1}{2}\beta\hbar\omega))$, which has the high-temperature expansion $k_B T \ln(\beta\hbar\omega) + k_B T [\frac{1}{24}(\beta\hbar\omega)^2 + O((\beta\hbar\omega)^4)]$, so that the harmonic free energy per atom of the vibrating crystal in the classical limit is

$$F_{\text{harm}} = \frac{3k_B T}{N_{\mathbf{k}s}} \sum_{\mathbf{k}s} \ln(\beta\hbar\omega_{\mathbf{k}s}), \quad (7)$$

where $\omega_{\mathbf{k}s}$ is the frequency of phonon branch s at wave vector \mathbf{k} and the sum goes over the first Brillouin zone, with $N_{\mathbf{k}s}$ the total number of k points and branches in the sum. It will be useful to express this in terms of the geometric average $\bar{\omega}$ of the phonon frequencies, defined as

$$\ln \bar{\omega} = \frac{1}{N_{\mathbf{k}s}} \sum_{\mathbf{k}s} \ln(\omega_{\mathbf{k}s}), \quad (8)$$

which allows us to write

$$F_{\text{harm}} = 3k_B T \ln(\beta\hbar\bar{\omega}). \quad (9)$$

The central quantity in the calculation of the frequencies is the force-constant matrix $\Phi_{ls\alpha, l't\beta}$, since the frequencies at wave vector \mathbf{k} are the eigenvalues of the dynamical matrix $D_{s\alpha, t\beta}$, defined as

$$D_{s\alpha, t\beta}(\mathbf{k}) = \frac{1}{M} \sum_{l'} \Phi_{ls\alpha, l't\beta} \exp[i\mathbf{k} \cdot (\mathbf{R}_{l't}^0 - \mathbf{R}_{ls}^0)], \quad (10)$$

where \mathbf{R}_{ls}^0 is the perfect-lattice position of atom s in primitive cell number l . If we have the complete force-constant matrix, then $D_{s\alpha, t\beta}$ and hence the frequencies $\omega_{\mathbf{k}s}$ can be obtained at any \mathbf{k} , so that $\bar{\omega}$ can be computed to any required precision. In principle, the elements of $\Phi_{ls\alpha, l't\beta}$ are nonzero for arbitrarily large separations $|\mathbf{R}_{l't}^0 - \mathbf{R}_{ls}^0|$, but in practice they decay rapidly with separation, so that a key issue in achieving our target precision is the cutoff distance beyond which the elements can be neglected.

We calculate $\Phi_{ls\alpha, l't\beta}$ by the small-displacement method, in a way similar to that described in Ref. 53. The basic principle is that $\Phi_{ls\alpha, l't\beta}$ describes the proportionality between displacements and forces. If the atoms are given small displacements $u_{ls\alpha}$ from their perfect-lattice positions, then to linear order the forces $F_{ls\alpha}$ are

$$F_{ls\alpha} = - \sum_{l't\beta} \Phi_{ls\alpha, l't\beta} u_{l't\beta}. \quad (11)$$

Within the *ab initio* scheme, all the elements $\Phi_{ls\alpha, l't\beta}$ are obtained for a given $l't\beta$ by introducing a small displacement $u_{l't\beta}$, all other displacements being zero, minimizing the electronic free energy, and evaluating all the forces $F_{ls\alpha}$. In practice, the displacement amplitude $u_{l't\beta}$ must be made small enough to ensure linearity to the required precision, and this sets the precision with which the electronic free energy must be minimized.

By translational symmetry, the entire force-constant matrix is obtained by making three independent displacements for each atom in the primitive cell, and this means that no more than $3N_{\text{bas}}$ calculations are needed, where N_{bas} is the number of atoms in the primitive cell. This number can be reduced by symmetry. If, as in the hcp crystal, all atoms in the primitive cell are equivalent under operations of the space group, then the entire force-constant matrix can be obtained by making at most three displacements of a single atom in the primitive cell: from $\Phi_{ls\alpha, l't\beta}$ for one chosen atom $l't$, one obtains $\Phi_{ls\alpha, l't\beta}$ for all other $l't$. Point-group symmetry reduces the number still further if linearly independent displacements of the chosen atom are equivalent by symmetry. This is the case in the hcp structure, since displacements in the basal plane related by rotations about the c axis by $\pm 120^\circ$ are equivalent by symmetry; this means that two calculations, one with the displacement along the c axis, and other with the displacement in the basal plane, suffice to obtain the entire $\Phi_{ls\alpha, l't\beta}$ matrix. The basal-plane displacement should be made along a symmetry direction, because the symmetry makes the calculations more efficient. Since the exact $\Phi_{ls\alpha, l't\beta}$ matrix has point-group symmetries, the calculated $\Phi_{ls\alpha, l't\beta}$ must be symmetrized to ensure that these symmetries are respected. The symmetrization also serves to eliminate the lowest-order nonlinearities in the relation between forces and displacements.⁵³

It is important to appreciate that the $\Phi_{ls\alpha, l't\beta}$ in the formula for $D_{s\alpha, t\beta}(\mathbf{k})$ is the force-constant matrix in the infinite lattice, with no restriction on the wave vector \mathbf{k} , whereas the *ab initio* calculations of $\Phi_{ls\alpha, l't\beta}$ can only be done in supercell geometry. Without a further assumption, it is strictly impossible to extract the infinite-lattice $\Phi_{ls\alpha, l't\beta}$ from supercell calculations, since the latter deliver information only at wavevectors that are reciprocal lattice vectors of the superlattice. The further assumption needed is that the infinite-lattice $\Phi_{ls\alpha, l't\beta}$ vanishes when the separation $\mathbf{R}_{l't} - \mathbf{R}_{ls}$ is such that the positions \mathbf{R}_{ls} and $\mathbf{R}_{l't}$ lie in different Wigner-Seitz (WS) cells of the chosen superlattice. More precisely, if we take the WS cell centered on $\mathbf{R}_{l't}$, then the infinite-lattice value of $\Phi_{ls\alpha, l't\beta}$ vanishes if \mathbf{R}_{ls} is in a different WS cell; it is equal to the supercell value if \mathbf{R}_{ls} is wholly within the same WS cell; and it is equal to the supercell value divided by an integer P if \mathbf{R}_{ls} lies on the boundary of the same WS cell, where P is the number of WS cells having \mathbf{R}_{ls} on their boundary. With this assumption, the $\Phi_{ls\alpha, l't\beta}$ elements will converge to the correct infinite-lattice values as the dimensions of the supercell are systematically increased.

D. Anharmonicity

1. Thermodynamic integration

Although we shall show that the anharmonic free energy F_{anharm} is numerically fairly small, it is far more challenging

to calculate than F_{perf} or F_{harm} , because there is no simple formula like Eq. (7), and the direct computation of the multidimensional integrals in the free-energy formulas such as Eq. (4) is impossible. Instead, we use the technique of thermodynamic integration (see, e.g., Ref. 54) to obtain the difference $F_{\text{vib}} - F_{\text{harm}}$, as developed in earlier papers.²⁻⁴

Thermodynamic integration is a completely general technique for determining the difference of free energies $F_1 - F_0$ for two systems whose total-energy functions are U_1 and U_0 . The basic idea is that $F_1 - F_0$ represents the reversible work done on continuously and isothermally switching the energy function from U_0 to U_1 . To do this switching, a continuously variable energy function U_λ is defined as

$$U_\lambda = (1 - \lambda)U_0 + \lambda U_1, \quad (12)$$

so that the energy goes from U_0 to U_1 as λ goes from 0 to 1. In classical statistical mechanics, the work done in an infinitesimal change $d\lambda$ is

$$dF = \langle dU_\lambda / d\lambda \rangle_\lambda d\lambda = \langle U_1 - U_0 \rangle_\lambda d\lambda, \quad (13)$$

where $\langle \cdot \rangle_\lambda$ represents the thermal average evaluated for the system governed by U_λ . It follows that

$$F_1 - F_0 = \int_0^1 d\lambda \langle U_1 - U_0 \rangle_\lambda. \quad (14)$$

In practice, this formula can be applied by calculating $\langle U_1 - U_0 \rangle_\lambda$ for a suitable set of λ values and performing the integration numerically. The average $\langle U_1 - U_0 \rangle_\lambda$ is evaluated by sampling over configuration space.

For the anharmonic free energy, a possible approach is to choose U_0 as U_{harm} and U_1 as U_{vib} , so that $F_1 - F_0$ is the anharmonic free energy F_{anharm} . This was the procedure used in our earlier *ab initio* work on the melting of Al,³ and a related technique was used by Sugino and Car² in their work on Si melting. However, the calculations are rather heavy, and the need for extensive sampling over the electronic Brillouin zone in the *ab initio* calculations makes it difficult to achieve high precision. We have now developed a more efficient two-step procedure, in which we go first from the harmonic *ab initio* system U_{harm} to an intermediate reference system U_{ref} which closely mimics the full *ab initio* total energy U_{vib} ; in the second step, we go from U_{ref} to U_{vib} . The anharmonic free energy is thus represented as

$$F_{\text{anharm}} = (F_{\text{vib}} - F_{\text{ref}}) + (F_{\text{ref}} - F_{\text{harm}}), \quad (15)$$

and the two differences are calculated by separate thermodynamic integrations:

$$F_{\text{vib}} - F_{\text{ref}} = \int_0^1 d\lambda \langle U_{\text{vib}} - U_{\text{ref}} \rangle_\lambda^{\text{vr}},$$

$$F_{\text{ref}} - F_{\text{harm}} = \int_0^1 d\lambda \langle U_{\text{ref}} - U_{\text{harm}} \rangle_\lambda^{\text{rh}}. \quad (16)$$

To distinguish clearly between these two parts of the calculation, we denote by $\langle \cdot \rangle_\lambda^{\text{rh}}$ the thermal average taken in the

ensemble generated by the switched total energy $U_\lambda^{\text{rh}} \equiv (1 - \lambda)U_{\text{harm}} + \lambda U_{\text{ref}}$ and by $\langle \cdot \rangle_\lambda^{\text{vr}}$ the corresponding average for $U_\lambda^{\text{vr}} \equiv (1 - \lambda)U_{\text{ref}} + \lambda U_{\text{vib}}$.

The crucial point of this is that U_{ref} is required to consist of an empirical model potential which quite accurately represents both the harmonic and anharmonic parts of the *ab initio* total energy U_{vib} . Since it is a model potential, the thermodynamic integration for $F_{\text{ref}} - F_{\text{harm}}$ can be performed with high precision on large systems. The difference $F_{\text{vib}} - F_{\text{ref}}$, by contrast, involves heavy *ab initio* calculations, but provided a good U_{ref} can be found these are manageable. The criterion for choosing a ‘‘good’’ U_{ref} is discussed in detail in the Appendix, and the reference system used in most of the present work is presented in Sec. II D 3.

2. Calculation of thermal averages

The calculation of thermal averages is just the standard problem of computational statistical mechanics, and can be accomplished by any method that allows us to draw unbiased samples of configurations from the appropriate ensemble. In this work, we employ molecular dynamics simulation. This means, for example, that to calculate $\langle U_{\text{ref}} - U_{\text{harm}} \rangle_\lambda^{\text{rh}}$ we generate a trajectory of the system using equations of motion derived from the total energy function U_λ^{rh} . In the usual way, an initial part of the trajectory is discarded for equilibration, and the remainder is used to estimate the average. The duration of this remainder must suffice to deliver enough *independent* samples to achieve the required statistical precision.

The key technical problem in calculating thermal averages in nearly harmonic systems is that of ergodicity. In the dynamical evolution of a perfectly harmonic system, energy is never shared between different vibrational modes, so that a system starting at any point in phase space fails to explore the whole of phase space. This means that in a nearly harmonic system exploration will be very slow and inefficient, and it is difficult to generate statistically independent samples. We solve this following Ref. 3: the statistical sampling is performed using Andersen molecular dynamics,⁵⁵ in which the atomic velocities are periodically randomized by drawing them from a Maxwellian distribution. This type of simulation generates the canonical ensemble and completely overcomes the ergodicity problem.

3. Reference system

As discussed in the Appendix, the computational effort needed to calculate $F_{\text{vib}} - F_{\text{ref}}$ is greatly reduced if the difference of total energies $U_{\text{vib}} - U_{\text{ref}}$ is small. More precisely, the criterion is that U_{ref} should be chosen so that the mean square fluctuations of $U_{\text{vib}} - U_{\text{ref}}$ are as small as possible. In fact, if the fluctuations are small enough, we can simply write $F_{\text{vib}} - F_{\text{ref}} \approx \langle U_{\text{vib}} - U_{\text{ref}} \rangle_{\text{ref}}$, with the average taken in the reference ensemble. If this is not good enough, the next approximation is readily shown to be

$$F_{\text{vib}} - F_{\text{ref}} \approx \langle U_{\text{vib}} - U_{\text{ref}} \rangle_{\text{ref}} - \frac{1}{2k_B T} \langle [U_{\text{vib}} - U_{\text{ref}} - \langle U_{\text{vib}} - U_{\text{ref}} \rangle_{\text{ref}}]^2 \rangle_{\text{ref}}. \quad (17)$$

The question of reference systems for Fe has already been discussed in our recent *ab initio* simulation work on the high-pressure liquid.³² We showed there that a remarkably good reference model is provided by a system interacting through inverse-power pair potentials:

$$U_{\text{IP}} = \frac{1}{2} \sum_{I \neq J} \phi(|\mathbf{R}_I - \mathbf{R}_J|), \quad (18)$$

where $\phi(r) = B/r^\alpha$, with B and α adjusted to minimize the fluctuations of the difference between U_{IP} and the *ab initio* energy. Unfortunately, we shall show that this is an unsatisfactory reference model for the solid, because the harmonic phonon dispersion relations produced by U_{IP} differ markedly from the *ab initio* ones. It is a particularly poor reference model at low temperatures where anharmonic corrections are small, because in that régime a good reference system must closely resemble U_{harm} . However, we find that U_{IP} becomes an increasingly good reference system as T approaches the melting temperature. We therefore adopt as a general form for the reference system a linear combination of U_{harm} and U_{IP} :

$$U_{\text{ref}} = c_1 U_{\text{harm}} + c_2 U_{\text{IP}}. \quad (19)$$

The coefficients c_1 and c_2 are adjusted to minimize the intensity of the fluctuations of $U_{\text{vib}} - U_{\text{ref}}$ for each thermodynamic state. The model for U_{IP} is exactly the same as in our work on the high-pressure liquid, with the parameters $\alpha = 5.86$ and B such that for $r = 2.0 \text{ \AA}$ $\phi(r) = 1.95 \text{ eV}$.

Now consider in more detail how this optimization of U_{ref} is to be done. In principle, the ensemble in which we have to sample the fluctuations of $U_{\text{vib}} - U_{\text{ref}}$ is the one generated by the continuously switched total energy $(1 - \lambda)U_{\text{ref}} + \lambda U_{\text{vib}}$ that governs the thermodynamic integration from U_{ref} to U_{vib} . In practice, this is essentially the same as sampling in either of the ensembles associated with U_{ref} or U_{vib} , provided the fluctuations of $U_{\text{vib}} - U_{\text{ref}}$ are indeed small. But even this poses a problem. We are reluctant to sample in the ensemble of U_{vib} , because extensive (and expensive) *ab initio* calculations are needed to achieve adequate statistical accuracy. On the other hand, we cannot sample in the ensemble of U_{ref} without knowing U_{ref} , which is what we are trying to find. We resolve this problem by constructing an initial optimized U_{ref} by minimizing the fluctuations in the ensemble of U_{harm} . We then use this initial U_{ref} to generate a new set of samples, which is then used to reoptimize U_{ref} . In principle, we should probably repeat this procedure until U_{ref} ceases to vary, but in practice we stop after the second iteration. Note that even this approach requires fully converged *ab initio* calculations for a large set of configurations. But since the configurations are generated with the potential model U_{ref} , statistically independent samples are generated with much less effort than if we were using U_{vib} to generate them.

III. THE RIGID PERFECT LATTICE

Our DFT calculations on the rigid perfect lattice give F_{perf} , and hence quantities such as electronic specific heat

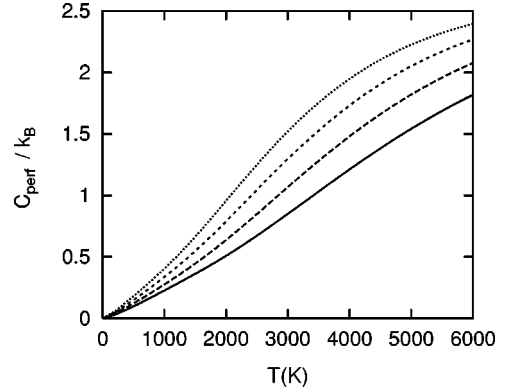


FIG. 1. Electronic specific heat per atom C_{perf} of the rigid perfect lattice of hcp Fe (units of Boltzmann's constant k_B) as a function of temperature for atomic volumes: 7.0 \AA^3 (—), 8.0 \AA^3 (---), 9.0 \AA^3 (- - -), and 10.0 \AA^3 (....).

C_{perf} and the pressure p_{perf} for any chosen volume and electronic temperature T_{el} . We do not discuss the low-temperature behavior, since there have already been many DFT studies of this.^{27–29,32} The various DFT calculations are in excellent accord, and reproduce accurately the low-temperature $p(V)$ relation measured in DAC experiments,⁹ especially at high pressures. The difference between the pressures calculated with the present PAW techniques and experimental values ranges from 9% at 100 GPa to 2.5% at 300 GPa, these deviations being only slightly greater than the scatter on the experimental values. Our results for the high-temperature thermodynamic properties of the rigid perfect lattice will be reported rather briefly, since they mainly confirm what is known in less detail from previous work.^{8,36}

All the calculations of this section employ the $15 \times 15 \times 9$ electronic Monkhorst-Pack set, which gives 135 k -points in the irreducible wedge of the Brillouin zone. Tests with finer k -point sets show that the residual k -point errors are less than 1 meV/atom for $T \geq 2000 \text{ K}$. We performed calculations of F_{perf} at a set of atomic volumes from 6.2 to 11.4 \AA^3 at intervals of 0.2 \AA^3 , and for every volume for T_{el} going from 200 to 10,000 K at intervals of 200 K. The calculations also deliver the internal energy E_{perf} and the electronic entropy S_{perf} , from which we obtain the specific heat either as $C_{\text{perf}} = (\partial E_{\text{perf}} / \partial T)_V$, or as $C_{\text{perf}} = T(\partial S_{\text{perf}} / \partial T)_V$ – consistency between the two methods provides a useful check.

Our results for C_{perf} are reported in Fig. 1 for the T_{el} range 0 – 6000 K at four atomic volumes. As expected from previous work,^{8,36,56} C_{perf} becomes large at high temperatures, its value of ca. $2k_B$ at 6000 K being comparable with the Dulong-Petit specific heat of lattice vibrations ($3k_B$), so that thermal electronic excitations are crucial to a correct description of Fe thermodynamics at core conditions. Our C_{perf} results are numerically quite close to those reported by Wasserman *et al.*,³⁶ though the latter actually refer to fcc Fe. The linear dependence of C_{perf} on T evident in Fig. 1 at low T [$C_{\text{perf}} = \gamma T + O(T^2)$] is expected from the standard Sommerfeld expansion⁵⁷ for electronic specific heat in powers of T , which shows that the low-temperature slope is given by $\gamma = \frac{1}{3} \pi^2 k_B^2 g(E_F)$, where $g(E_F)$ is the electronic density of

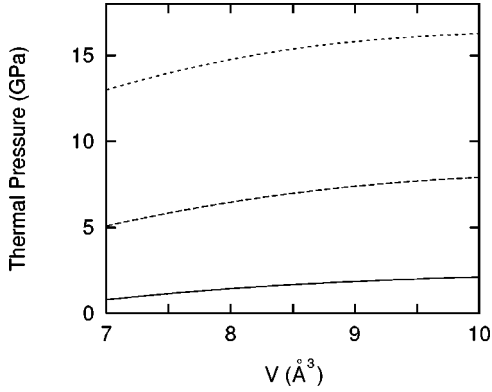


FIG. 2. Electronic thermal pressure Δp_{perf} of the rigid perfect lattice of hcp Fe as a function of atomic volume V for $T=2000$ (—), 4000 (---), and 6000 K (- · -).

states (DOS, i.e., the number of states per unit energy per atom) at the Fermi energy E_F . We have made separate calculations of the DOS and obtained γ from $g(E_F)$, which give a useful cross-check on the low-temperature slope of C_{perf} .

In order to obtain other thermodynamic functions, we need a fit to our F_{perf} results. At each temperature, we fit the results to the standard Birch-Murnaghan form, using exactly the procedure followed in our recent work on the Fe/O system.³⁵ This involves fitting the 22 values of F_{perf} at a given temperature using four fitting parameters (E_0 , V_0 , K and K' in the notation of Ref. 35). We find that at all temperatures the rms fitting errors are less than 1 meV at all points. The temperature variation of the fitting parameters is then represented using a polynomial of sixth degree.

Electronic excitations have a significant effect on the pressure, as can be seen by examining the T dependence of the perfect-lattice pressure $p_{\text{perf}} = -(\partial F_{\text{perf}}/\partial V)_T$. We display in Fig. 2 the thermal part Δp_{perf} of p_{perf} , i.e., the difference between p_{perf} at a given T and its zero-temperature value. The thermal excitation of electrons produces a positive pressure. This is what intuition would suggest, but it is worth noting the reason. Since $F_{\text{perf}}(T_{\text{el}}) = F_{\text{perf}}(0) - \frac{1}{2}T^2\gamma(V)$ at low temperatures, the change of pressure due to electronic excitations is $\Delta p = \frac{1}{2}T^2 d\gamma/dV$ in this region. But $d\gamma/dV > 0$, so that the electronic thermal pressure must

be positive. To put the magnitude of this pressure in context, we recall that at the Earth's inner-core boundary (ICB) the pressure is 330 GPa and the temperature is believed to be in the range 5000–6000 K, the atomic volume of Fe under these conditions being ca. 7 \AA^3 . Our results then imply that electronic thermal pressure accounts for ca. 4 % of the total pressure, which is small but significant.

IV. THE HARMONIC CRYSTAL

A. Convergence tests

We have made extensive tests to ensure that our target precision of 10 meV/atom is attained for the harmonic free energy F_{harm} . We note that at 6000 K this requires that the geometric mean frequency $\bar{\omega}$ be calculated with a precision of 0.7%. Convergence of $\bar{\omega}$ must be achieved with respect to four main parameters: the atomic displacement used to calculate the force-constant matrix $\Phi_{ls\alpha, l't\beta}$; the electronic k -point sampling; the size of the repeating cell used to obtain $\Phi_{ls\alpha, l't\beta}$; and the density of the k -point mesh used in calculating $\bar{\omega}$ from $\omega_{\mathbf{k}s}$ by integration over the phonon Brillouin zone [see Eq.(7)].

The technical measures taken to achieve convergence are as follows. Integration over the phonon Brillouin zone was performed using 364 Monkhorst-Pack k -points in the irreducible wedge, and an atomic displacement amplitude of 0.0148 \AA was used; the associated errors in F_{harm} are less than 1 meV/atom in both cases. For electronic k -point sampling, we use the $5 \times 5 \times 5$ Monkhorst-Pack set, which reduces k -point errors to less than 0.1 meV/atom at all temperatures T_{el} of interest. Finally, we tested the convergence of F_{harm} with respect to the size of repeating cell used to generate $\Phi_{ls\alpha, l't\beta}$, going up to cells containing 150 atoms. We found that with the $3 \times 3 \times 2$ repeating cell the error in F_{harm} calculated at the atomic volume $V=8.67 \text{ \AA}^3$ and $T=4300 \text{ K}$ is a little over 2 meV/atom, and we adopted this cell size for all the calculations.

B. Dispersion relations, average frequency, free energy

In Fig. 3 we present the harmonic phonon dispersion relations at the two atomic volumes 8.67 and 6.97 \AA^3 calculated with $T_{\text{el}}=4000 \text{ K}$. We are not aware of previous direct *ab initio* calculations of the phonon frequencies of high-

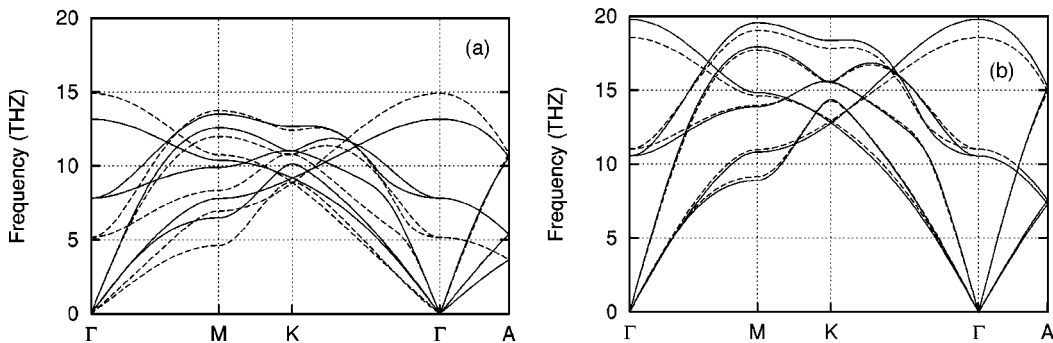


FIG. 3. Phonon dispersion relations of hcp Fe calculated at atomic volumes $V=8.67$ (left panel) and 6.97 \AA^3 (right panel). Frequencies calculated directly from DFT at the two volumes are shown as solid curves. In left panel, dashed curves give frequencies from empirical inverse-power model (see text). In right panel, dashed curves show DFT frequencies for $V=8.67 \text{ \AA}^3$ graphed in left panel but scaled by the factor 1.409.

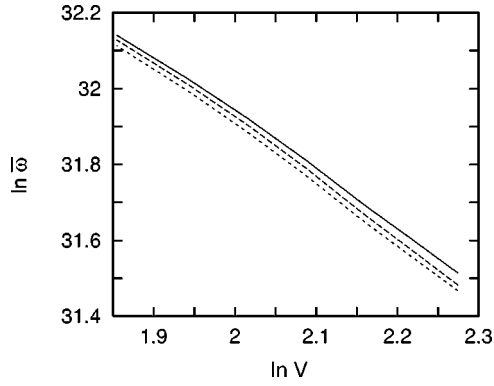


FIG. 4. Geometric-mean phonon frequency $\bar{\omega}$ of hcp Fe as a function of atomic volume V for $T=2000$ (—), 4000 (---), and 6000 K (- - -). The natural logarithm of the two quantities is plotted, with $\bar{\omega}$ in units of rad s^{-1} and V in units of \AA^3 .

pressure hcp Fe, but there are published dispersion relations derived from a “generalized pseudopotential” parameterization of FP-LMTO calculations performed by Söderlind *et al.*²⁸ using the LDA at the atomic volume 6.82 \AA^3 . The agreement of their phonon frequencies with ours is far from perfect. For example, we find that the maximum frequency in the Brillouin zone calculated at $V=6.82 \text{ \AA}^3$ is at the Γ -point and is 21.2 THz , whereas they find the maximum frequency at the M -point with the value 17.2 THz . This is not unexpected, since they report that the generalized pseudopotential scheme fails to reproduce accurately some phonon frequencies calculated directly with FP-LMTO in the fcc Fe crystal;²⁸ in addition, the LDA used by them is known to underestimate phonon frequencies in Fe.²⁹

Casual inspection suggests that our dispersion curves at the two atomic volumes are almost identical apart from an overall scale factor. This suggestion can be judged from the right-hand panel of Fig. 3, where we plot as dashed curves the dispersion curves at $V=8.67 \text{ \AA}^3$ scaled by the factor 1.409 —the reason for choosing this factor will be explained below. The comparison shows that the curves at the two volumes are indeed related by a single scaling factor to within ca. 5%. We also take the opportunity here to check how well the inverse-power potential model U_{IP} [see Eq. (18)] reproduces phonon frequencies. To do this, we take exactly the same parameters B and α specifying $\phi(r)$ that reproduced well the properties of the liquid,³² namely $\alpha=5.86$ and B such that for $r=2.0 \text{ \AA}$ $\phi(r)=1.95 \text{ eV}$. The phonons calculated from this model are compared with the *ab initio* phonons at atomic volume $V=8.67 \text{ \AA}^3$ in the left panel of Fig. 3. Although the general form of the dispersion curves is correctly reproduced, it is clear that the model gives only a very rough description, with discrepancies of as much as 30% for some frequencies.

We performed direct *ab initio* calculations of the dispersion relations and hence the geometric mean frequency $\bar{\omega}$ for seven volumes spaced roughly equally from 9.72 to 6.39 \AA^3 , and for each of these volumes for T_{el} from 1000 to $10,000 \text{ K}$ at intervals of 500 K . The results for $\bar{\omega}$ as function of volume are reported in Fig. 4 for the three temperatures $T_{\text{el}}=2000$,

4000 , and 6000 K . We use a (natural) log-log plot to display the results, so that the negative slope $\gamma_{\text{ph}} \equiv -d \ln \bar{\omega} / d \ln V$ is the so-called phonon Grüneisen parameter. (The relation between γ_{th} and the thermodynamic Grüneisen parameter γ will be discussed in Sec. VI B.) We note that if phonon dispersion curves at two different volumes are related by a simple scaling factor, this must be the ratio of $\bar{\omega}$ values at the two volumes. The scaling factor used in Fig. 3 was obtained in exactly this way from our $\bar{\omega}$ results. The Grüneisen parameter γ_{ph} increases with increasing volume, in accord with a widely used rule of thumb.⁵⁸ We find that γ_{ph} goes from 1.34 at $V=6.7 \text{ \AA}^3$ to 1.70 at $V=8.3 \text{ \AA}^3$, but then decreases slightly to 1.62 at $V=9.5 \text{ \AA}^3$. Figure 3 also allows us to judge the effect of T_{el} on phonon frequencies: for all volumes studied, the frequencies decrease by ca. 4% as T_{el} goes from 2000 to 6000 K . However, we mention that for the higher volumes, though not for the smaller ones, $\bar{\omega}$ slightly increases again as T_{el} goes to still higher values. To enable the $\bar{\omega}$ data to be used in thermodynamic calculations, we parameterize the temperature dependence of $\ln \bar{\omega}$ at each volume as $a + bT^2 + cT^3 + eT^5$, and the volume dependence of the four coefficients a , b , c and e as a third-degree polynomial in V .

We now return to the matter of quantum nuclear corrections. Since the leading high-temperature correction to the free energy is $\frac{1}{24} k_{\text{B}} T (\beta \hbar \omega)^2$ per mode and there are three modes per atom, the quantum correction to F_{harm} is $\frac{1}{8} k_{\text{B}} T (\beta \hbar \langle \omega^2 \rangle^{1/2})^2$ per atom, where $\langle \omega^2 \rangle$ denotes the average of ω^2 over wavevectors and branches. At the lowest volume of interest, $V=7 \text{ \AA}^3$, $\langle \omega^2 \rangle^{1/2} / 2\pi$ is roughly 15 THz . At the lowest temperature of interest, $T=2000 \text{ K}$; this gives a quantum correction of 3 meV/atom , which is small compared with our target precision.

C. Harmonic phonon specific heat and thermal pressure

If the mean frequency $\bar{\omega}$ were independent of temperature, the constant-volume specific heat C_{harm} due to harmonic phonons would be exactly $3k_{\text{B}}$ per atom in the classical limit employed here. We find that its temperature dependence yields a slight increase of C_{harm} above this value, but this is never greater than $0.25k_{\text{B}}$ under the conditions of interest. The harmonic phonon pressure p_{harm} as a function of atomic volume at different temperatures is reported in Fig. 5. Comparison with Fig. 2 shows that p_{harm} is always much bigger (by a factor of at least three) than the electronic thermal pressure under the conditions of interest. At ICB conditions ($p=330 \text{ GPa}$, $T \sim 5000\text{--}6000 \text{ K}$), p_{harm} account for ca. 15% of the total pressure.

V. ANHARMONIC FREE ENERGY

A. Optimization of reference system

It is stressed in Sec. II D 3 and in the Appendix that optimization of the reference system greatly improves the efficiency of the anharmonic calculations. We investigated the construction of the reference system in detail at the atomic

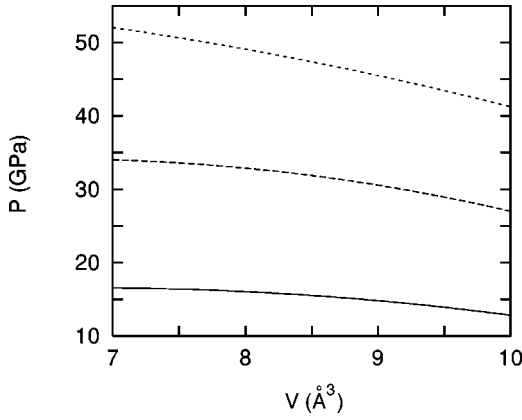


FIG. 5. The harmonic thermal pressure p_{harm} as a function of atomic volume V for $T=2000$ (—), 4000 (- - -), and 6000 K (- · -).

volume 8.67 \AA^3 , with the optimizations performed for a simulated system of 16 atoms. The calculation of the anharmonic free energy itself for a system as small as this would not be adequate, but we expect this system size to suffice for the optimization of U_{ref} . The initial sample of configurations (see Sec. II D 3) was taken from a simulation of duration 100 ps performed with the total energy U_{harm} , with velocity randomization typically every 0.2 ps. Configurations were taken every 1 ps, so that we obtain a sample of 100 configurations. In computing the energy difference $U_{\text{vib}} - U_{\text{ref}}$ for these configurations, the *ab initio* energy U_{vib} was always computed using $5 \times 5 \times 3$ Monkhorst-Pack electronic k -point sampling (38 k -points in the full Brillouin zone). Once the preliminary optimization had been performed with configurations generated like this, the resulting U_{ref} was used to produce a new set of 100 configurations with an Andersen MD simulation of the same duration as before, and the reference system was reoptimized.

This entire procedure was carried out at temperatures of 1000 and 4000 K. The values of the optimization coefficients [see Eq. (19)] were $c_1=0.2$, $c_2=0.8$ at the high temperature and $c_1=0.7$, $c_2=0.3$ at the low temperature. (We do not require that $c_1+c_2=1$, though this happens to be the case here.) As expected, U_{ref} resembles U_{harm} quite closely at the low temperature and U_{IP} quite closely at the high temperature.

In view of the labor involved in the optimization, we wanted to find out whether the detailed choice of c_1 and c_2 makes a large difference to the strength of the fluctuations of $U_{\text{vib}} - U_{\text{ref}}$, which can be characterized by the quantity $Q = [\langle \delta \Delta U^2 \rangle / N]^{1/2}$, where $\delta \Delta U = \Delta U - \langle \Delta U \rangle$, with $\Delta U = U_{\text{vib}} - U_{\text{ref}}$. To do this, we computed these fluctuations at several temperatures, using the reference models just described, i.e., without optimizing the c_i coefficients at each temperature. We find that with $c_1=0.2$, $c_2=0.8$ the quantity Q has very small values in the range $0.05-0.09$ eV in all cases, and we therefore used this way of making the reference system in all subsequent calculations.

B. From harmonic *ab initio* to reference to full *ab initio*

The thermodynamic integration from *ab initio* harmonic to reference was done with nine equally-spaced λ -points us-

ing Simpson's rule, which gives an integration precision well in excess of our target. To investigate the influence of system size, integration from U_{harm} to U_{ref} was performed for systems of 12 different sizes, going from 16 to 1200 atoms. The calculations were also repeated with the force-constant matrix in U_{harm} generated with cells containing from 16 to 150 atoms (see Sec. II C). These tests showed that if the thermodynamic integration is done with a system of 288 atoms and the force constant used for U_{harm} is generated with the 36-atom cell, then the resulting difference $F_{\text{ref}} - F_{\text{harm}}$ is converged to better than 3 meV/atom.

To compute the difference $F_{\text{vib}} - F_{\text{ref}}$, we used the second-order expansion formula given in Eq. (17). Given the small size of the fluctuations of $U_{\text{vib}} - U_{\text{ref}}$, we expect this to be very accurate. The calculations of $F_{\text{vib}} - F_{\text{ref}}$ were all done with the 16-atom system. Tests with 36- and 64-atom systems show that this free-energy difference is converged with respect to size effects to within ca. 2 meV.

In classical statistical mechanics, F_{anharm} is expected to go as T^2 at low temperatures, and in fact we find that our results for F_{anharm} are well represented by $F_{\text{anharm}} = a(V)T^2$ for all the temperatures studied. The volume dependence of $a(V)$ is adequately represented by $a(V) = \alpha_1 + \alpha_2 V$, with $\alpha_1 = 1.8 \times 10^{-9} \text{ eV K}^{-2}$ and $\alpha_2 = -4.8 \times 10^{-10} \text{ eV \AA}^{-3} \text{ K}^{-2}$ per atom. This means that for the atomic volumes of interest the anharmonic free energy is always negative, so that anharmonicity stabilizes the solid. The temperature at which anharmonicity becomes appreciable is higher for smaller atomic volumes.

C. Anharmonic specific heat and pressure

Within the parametrization just described, the anharmonic contribution to the constant-volume specific heat C_{anharm} is proportional to T and varies linearly with V . As an indication of its general size, we note that C_{anharm} increases from 0.09 to $0.18 k_B$ at 2000 K and from 0.28 to $0.53 k_B$ at 6000 K as V goes from 7 to 10 \AA^3 . The anharmonic contribution to the pressure is independent of volume, and is proportional to T^2 . It increases from 0.4 to 3.5 GPa as T goes from 2000 to 6000 K, so that even at high temperatures it is barely significant.

VI. THERMODYNAMICS OF THE SOLID

We now combine the parametrized forms for F_{perf} , F_{harm} , and F_{anharm} presented in the previous three sections to obtain the total free energy of the hcp crystal, and hence, by taking appropriate derivatives, a range of other thermodynamic functions, starting with those measured in shock experiments.

A. Thermodynamics on the Hugoniot

In a shock experiment, conservation of mass, momentum and energy requires that the pressure p_H , the molar internal energy E_H , and the molar volume V_H in the compression wave are related by the Rankine-Hugoniot formula:⁶⁰

$$\frac{1}{2} p_H (V_0 - V_H) = E_H - E_0, \quad (20)$$

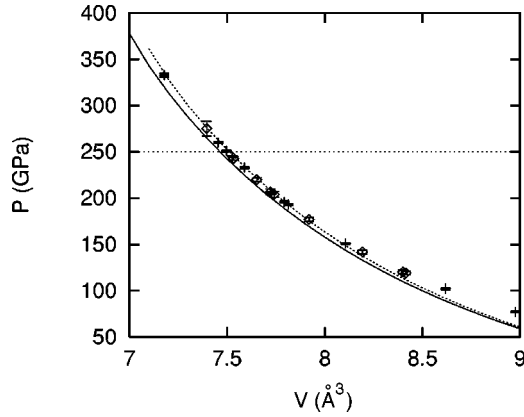


FIG. 6. Experimental and *ab initio* Hugoniot pressure p as a function of atomic volume V . Symbols show the measurements of Brown and McQueen (Ref. 21). Solid curve is *ab initio* pressure obtained when calculated equilibrium volume of bcc Fe is used in the Hugoniot-Rankine equation; dotted curve is the same, but with experimental equilibrium volume of bcc Fe. The comparison is meaningful only up to a pressure of ca. 250 GPa (horizontal dotted line), at which point the experiments indicate melting.

where E_0 and V_0 are the internal energy and volume in the zero-pressure state before the arrival of the wave. The quantities directly measured are the shock-wave and material velocities, which allow the values of p_H and V_H to be deduced. From a series of experiments, p_H as a function of V_H (the so-called Hugoniot) can be derived. The measurement of temperature in shock experiments is attempted but problematic.²²

The Hugoniot curve $p_H(V_H)$ is straightforward to compute from our results: for a given V_H , one seeks the temperature at which the Rankine-Hugoniot relation is satisfied; from this, one obtains p_H (and, if required, E_H). In experiments on Fe, V_0 and E_0 refer to the zero-pressure bcc crystal, and we obtain their values directly from GGA calculations, using exactly the same PAW technique and GGA as in the rest of the calculations. Since bcc Fe is ferromagnetic, spin polarization must be included, and this is treated by spin interpolation of the correlation energy due to Vosko *et al.*,⁵⁹ as described in Refs. 32 and 41. The value of E_0 includes the harmonic vibrational energy at 300 K, calculated from *ab initio* phonon dispersion relations for ferromagnetic bcc Fe.

Our *ab initio* Hugoniot is compared with the measurements of Brown and McQueen²¹ in Fig. 6. The agreement is good, with discrepancies ranging from 10 GPa at $V = 7.8 \text{ \AA}^3$ to 12 GPa at $V = 8.6 \text{ \AA}^3$. These discrepancies are only slightly greater than those found for the room-temperature static $p(V)$ curve (see Sec. III), which can be regarded as giving an indication of the intrinsic accuracy of the GGA itself. Another way of looking at the accuracy to be expected of the GGA is to recalculate the Hugoniot using the experimental value of the bcc V_0 (11.8 \AA^3 , compared with the *ab initio* value of 11.55 \AA^3). The Hugoniot calculated in this way is also plotted in Fig. 6, and we see that this gives almost perfect agreement with the experimental data in the pressure range 100–240 GPa. We deduce from this that the *ab initio* Hugoniot deviates from the experimental data by an

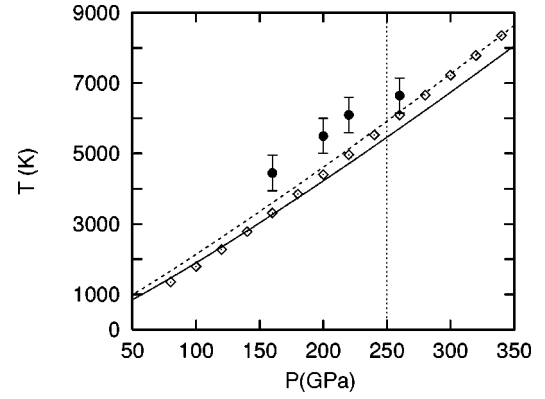


FIG. 7. Experimental and *ab initio* temperature as a function of pressure on the Hugoniot. Black circles with error bars and white diamonds are measurements due to Yoo *et al.* (Ref. 22) and estimates due to Brown and McQueen (Ref. 21), respectively. Solid and dashed curves are *ab initio* results obtained using theoretical and experimental bcc volumes. The comparison is meaningful only up to a pressure of ca. 250 GPa (vertical dotted line), at which point the experiments indicate melting.

amount which should be expected from the known inaccuracies of the GGA applied to Fe. A similar comparison with the experimental Hugoniot was given in the tight-binding total-energy work of Wasserman *et al.*,³⁶ and their agreement was as good as ours. We discuss the significance of this later.

Our Hugoniot temperature as function of pressure is compared with the experimental results of Yoo *et al.*²² in Fig. 7. We also include in the figure the estimates for Hugoniot temperature due to Brown and McQueen.²¹ The latter estimates were based on the basic thermodynamic relation:²¹

$$dT = -T(\gamma/V) dV + [(V_0 - V) dP + (P - P_0) dV] / (2C_v) \quad (21)$$

between infinitesimal changes of dT , dV , and dP along the Hugoniot. This relation contains the constant-volume specific heat C_v and the Grüneisen parameter γ , for which Brown and McQueen had to make assumptions. Our *ab initio* temperatures fall substantially below those of Yoo *et al.*, and this supports the suggestion of Ref. 36 that the Yoo *et al.* measurements overestimate the Hugoniot temperature by ca. 1000 K. On the other hand, our temperatures agree rather closely with the Brown and McQueen estimates. When we examine (Sec. VI B) their assumptions about C_v and γ , we shall see that they were reasonable, though the agreement between their temperatures and ours is also partly due to cancellation of errors between terms in Eq. (21).

A further quantity that can be extracted from shock experiments is the bulk sound velocity v_B as a function of atomic volume on the Hugoniot, which is given by $v_B = (K_S/\rho)^{1/2}$, with $K_S \equiv -V(\partial p/\partial V)_S$ the adiabatic bulk modulus and ρ the mass density. Since K_S can be calculated from our *ab initio* pressure and entropy as functions of V and T , our calculated K_S can be directly compared with experimental values (Fig. 8). Here, there is a greater discrepancy than one would wish, with the theoretical values falling significantly above the K_S values of both Refs. 21 and 20, al-

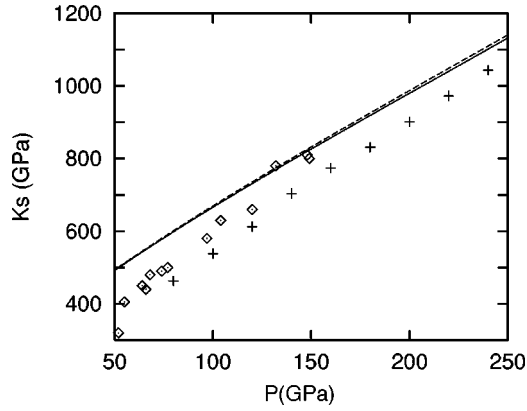


FIG. 8. Experimental and *ab initio* adiabatic bulk modulus K_S on the Hugoniot. Diamonds and pluses are measurements due to Jeanloz (Ref. 20) and Brown and McQueen (Ref. 21), respectively. Solid and dashed curves are *ab initio* results obtained using theoretical and experimental bcc volumes.

though we note that the two sets of experimental results disagree by an amount comparable with the discrepancy between theory and experiment.

For what it is worth, we show in Fig. 9 a comparison between our calculated thermal expansivity on the Hugoniot with values extracted from shock data by Jeanloz.²⁰ The latter are very scattered, but it is clear that the theoretical values have similar magnitude. However, our values vary little along the Hugoniot, whereas the experimental values seem to decrease rather rapidly with increasing pressure.

B. Other thermodynamic quantities

We conclude our presentation of results by reporting our *ab initio* predictions of quantities which characterize hcp Fe at high pressures and temperatures, and allow some further comparisons with the predictions of Refs. 8 and 36. Our results are presented as a function of pressure on isotherms at $T=2000$, 4000, and 6000 K. At each temperature, we give results only for the pressure range where, according to our preliminary *ab initio* melting curve,⁴³ the hcp phase is ther-

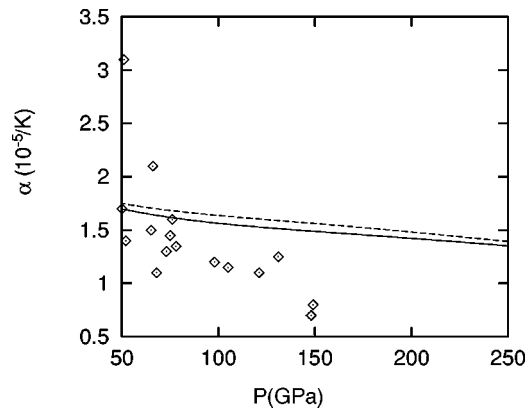


FIG. 9. Experimental and *ab initio* thermal expansivity on the Hugoniot. Diamonds are measurements due to Jeanloz (Ref. 20). Solid and dashed curves are *ab initio* results obtained using theoretical and experimental bcc volumes.

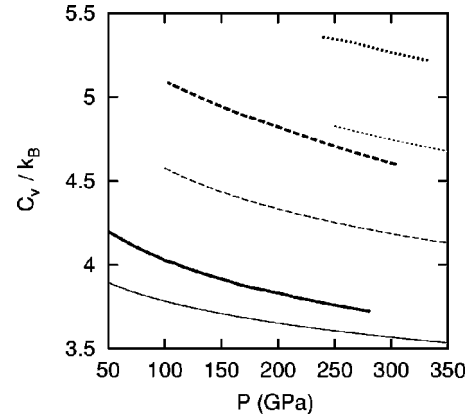


FIG. 10. Total constant-volume specific heat per atom C_v (units of k_B) of hcp Fe as a function of pressure on isotherms $T=2000$ K (continuous curves), 4000 K (dashed curves), and 6000 K (dotted curves). Heavy and light curves show present results and those of Refs. 8 and 36, respectively.

modynamically stable. In comparing with the predictions of Refs. 8 and 36, we use the explicit numerical results from Ref. 36 for thermodynamic quantities on the 2000 K isotherm. For the higher temperatures, we rely on the approximate parametrized formulas given in Ref. 8.

The total constant-volume specific heat per atom C_v (Fig. 10) emphasizes again the importance of electronic excitations. In a purely harmonic system, C_v would be equal to $3k_B$, and it is striking that C_v is considerably greater than that even at the modest temperature of 2000 K, while at 6000 K it is nearly doubled. The decrease of C_v with increasing pressure evident in Fig. 10 comes from the suppression of electronic excitations by high compression, and to a smaller extent from the suppression of anharmonicity. We note that our C_v values are significantly higher than those of Refs. 8 and 36; the main reason for this seems to be our inclusion of anharmonic corrections and the T -dependence of harmonic frequencies.⁶¹ Brown and McQueen²¹ made assumptions about the high- p /high- T behavior of C_v in order to estimate the Hugoniot temperature (see above Sec. VI A). Their assumptions were that the lattice contribution to C_v is equal to $3R$ above the Debye temperature and that the electronic contribution can be represented in the form $\beta_e(V/V_{\text{ref}})^{\gamma_e}T$, where V_{ref} is a reference density, and β_e and γ_e are constants whose values were taken from earlier theoretical calculations.⁵⁶ Since anharmonic and electronic contributions are negligible at low temperatures, our calculated C_v agrees with the Brown-McQueen values on the low- p /low- T part of the Hugoniot. However, our C_v rises slightly faster, mainly because of anharmonicity, and becomes ca. 3% higher than theirs at 200 GPa, the difference between the two decreasing again thereafter.

The thermal expansivity α (Fig. 11) is one of the few cases where we can compare with DAC measurements.¹⁰ The latter show that α decreases strongly with increasing pressure and our *ab initio* results fully confirm this. Our results also show that α increases significantly with temperature. Both trends are also shown by the calculations of Refs.

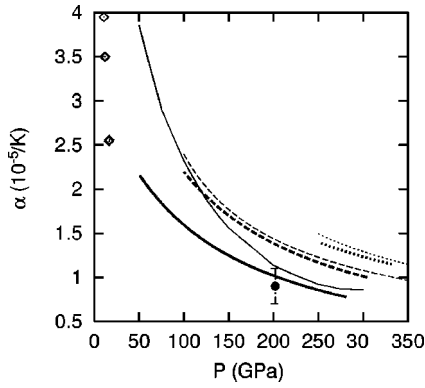


FIG. 11. Thermal expansivity α of hcp Fe as a function of pressure on isotherms $T=2000$ K (continuous curves), 4000 K (dashed curves), and 6000 K (dotted curves). Heavy and light curves show present results and those of Refs. 8 and 36, respectively. Black circle with error bar is experimental value of Duffy and Ahrens (Ref. 62) at $T=5200\pm 500$ K. Diamonds are DAC values due to Boehler¹⁰ for temperatures between 1500 and 2000 K.

8 and 36, though the latter differ from ours in showing considerably larger values of α at low pressure and temperature.

The product αK_T of expansivity and isothermal bulk modulus, which is equal to $(\partial p/\partial T)_v$, is important because it is sometimes assumed to be independent of pressure and temperature over a wide range of conditions, and this constancy is used to extrapolate experimental data. Our predicted isotherms for αK_T (Fig. 12) indicate that its dependence on p is indeed weak, especially at low temperatures, but that its dependence on T certainly cannot be ignored, since it increases by at least 30% as T goes from 2000 to 6000 K at high pressures. Wasserman *et al.*³⁶ come to qualitatively similar conclusions, and they also find values of ca. 10 MPa K⁻¹ at $T\approx 2000$ K. However, we note that the general tendency in our results for αK_T to increase with pressure at low pressures is not found in the results of Ref. 36 at 2000 K. In particular, they found a marked increase of αK_T with decreasing p , which does not occur in our results.

The thermodynamic Grüneisen parameter $\gamma \equiv V(\partial p/\partial E)_v \equiv \alpha K_T V/C_v$ plays an important role in high-

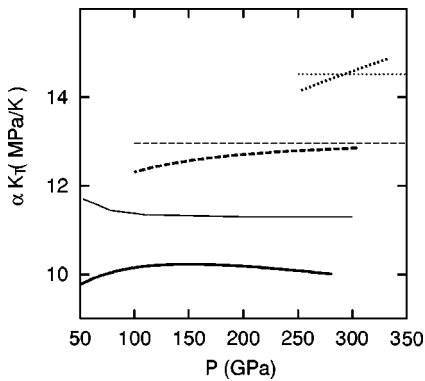


FIG. 12. Product of expansion coefficient α and isothermal bulk modulus K_T as a function of pressure on isotherms $T=2000$ K (continuous curves), 4000 K (dashed curves), and 6000 K (dotted curves). Heavy and light curves show present results and those of Refs. 8 and 36, respectively.

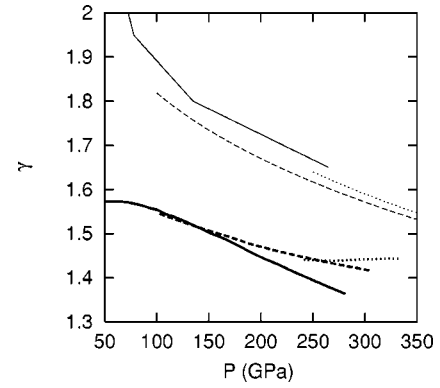


FIG. 13. Grüneisen parameter γ as a function of pressure on isotherms at $T=2000$ K (continuous curves), 4000 K (dashed curves), and 6000 K (dotted curves). Solid and light curves show present results and those of Refs. 8 and 36, respectively.

pressure physics, because it relates the thermal pressure (i.e., the difference p_{th} between p at given V and T and p at the same V but $T=0$) and the thermal energy (difference E_{th} between E at given V and T and E at the same V but $T=0$). Assumptions about the value of γ are frequently used in reducing shock data from Hugoniot to isotherm. If one assumes that γ depends only on V , then the thermal pressure and energy are related by

$$p_{\text{th}}V = \gamma E_{\text{th}}, \quad (22)$$

a relation known as the Mie-Grüneisen equation of state. At low temperatures, where only harmonic phonons contribute to E_{th} and p_{th} , γ should indeed be temperature independent above the Debye temperature, because $E_{\text{th}}=3k_B T$ per atom, and $p_{\text{th}}V = -3k_B T d \ln \bar{\omega}/d \ln V = 3k_B T \gamma_{\text{th}}$, so that $\gamma = \gamma_{\text{ph}}$, which depends only on V . But in high-temperature Fe, the temperature independence of γ will clearly fail, because of electronic excitations (and anharmonicity).

Our results for γ (Fig. 13) indicate that it varies rather little with either pressure or temperature in the region of interest. At temperatures below ca. 4000 K, it decreases with increasing pressure, as expected from the behavior of the phonon Grüneisen parameter γ_{ph} (see Sec. IV B). This is also expected from the often-used empirical rule of thumb⁵⁸ $\gamma \approx (V/V_0)^q$, where V_0 is a reference volume and q is a constant exponent usually taken to be roughly unity. Since V decreases by a factor of about 0.82 as p goes from 100 to 300 GPa, this empirical relation would make γ decrease by the same factor over this range, which is roughly what we see. However, the pressure dependence of γ is very much weakened as T increases, until at 6000 K γ is almost constant. Our results agree moderately well with those of Refs. 8 and 36 in giving a value $\gamma \approx 1.5$ at high pressures, but at low pressures there is a significant disagreement, since they find a strong increase of γ to values of over 2.0 as $p \rightarrow 0$, whereas our values never exceed 1.6 .

In making their estimates of the Hugoniot temperature, Brown and McQueen²¹ assumed that $(\partial E/\partial p)_v = V/\gamma$ is a constant equal to 2.85×10^{-6} m³ mol⁻¹. This implies that γ is ca. 2.2 on the low- p /low- T part of the Hugoniot,

whereas our calculations give ca. 1.5. However, with increasing pressure, the Brown-McQueen value of γ approaches ours, being only ca. 8% higher at 200 GPa. Given the differences between their C_v and γ values and ours, one might expect a larger disagreement between their Hugoniot temperatures and ours (Sec. VI A). However, it turns out that there is some cancellation between the differences in the various terms of Eq. (21) which brings the temperature curves into the quite close agreement that we have seen (Fig. 7).

VII. DISCUSSION AND CONCLUSIONS

Our primary interest in this work is in the properties of hcp iron at high pressures and temperatures, but in order to investigate them using *ab initio* methods we have needed to make technical developments, which have a wider significance. The major technical achievement is that we have been able to calculate the *ab initio* free energy and other thermodynamic properties with completely controlled statistical-mechanical errors, i.e., errors that can be reduced to any required extent. Anharmonicity and thermal electronic excitations are fully included. The attainment of high precision for the electronic and harmonic parts of the free energy has required no particular technical innovations, though careful attention to sources of error is essential. The main innovation is in the development of well optimized reference systems for use with thermodynamic integration in the calculation of the anharmonic part, without which adequate precision would be impossible. With the methods we have developed, it becomes unnecessary to approximate the electronic structure with semiempirical representations, or to resort to the statistical-mechanical approximations that have been used in the past.

We have assessed in detail the precision achieved in the various parts of the free energy. There are two kinds of errors: those incurred in the calculation of the free energies themselves, and those produced by fitting the results to polynomials. We have seen that the errors in calculating the perfect-lattice free energy F_{perf} are completely negligible, though there may be small fitting errors of perhaps 1 meV/atom. In the harmonic part F_{harm} , the calculational errors are ca. 3 meV/atom, most of which comes from spatial truncation of the force-constant matrix; the fitting error for F_{harm} are of about the same size. The most serious errors are in the anharmonic part F_{anharm} , and these are ca. 5 meV/atom in the calculation and ca. 4 meV/atom in the fitting. The overall technical errors therefore amount to ca. 15 meV/atom, which is slightly larger than our target of 10 meV/atom.

We stress that the precision just quoted does not take into account errors incurred in the particular implementation of DFT (PAW in the present work), for example the error associated with the chosen split between valence and core states. Such errors can in principle be systematically reduced, but we have not attempted this here. Nor does it account for the inaccuracy of the chosen E_{xc} , or for the neglect of the temperature dependence of E_{xc} .

The most direct way to test the reliability of our methods is comparison with shock data for $p(V)$ on the Hugoniot,²¹

so it is gratifying to find close agreement over the pressure range of interest. The closeness of this agreement is inherently limited by the known inaccuracies of the GGA employed, and we have shown that the discrepancies are of the expected size. An important prediction of the calculations is the temperature $T(p)$ on the Hugoniot, since temperature is notoriously difficult to obtain in shock experiments. Our results support the reliability of the shock temperatures estimated by Brown and McQueen,²¹ and, in agreement with Wasserman *et al.*,³⁶ we find that the temperatures of Yoo *et al.*²² are too high by as much as 1000 K. This incidentally lends support to the reliability of the Brown and McQueen estimate of ca. 5500 K for the melting temperature of Fe at 243 GPa. The situation is not so satisfactory for the adiabatic bulk modulus K_S on the Hugoniot, since our *ab initio* values seem to be ca. 8% above the shock values. But it should be remembered that even at ambient conditions *ab initio* and experimental bulk moduli frequently differ by this amount. The difficulties may be partly on the experimental side, since even for bcc Fe at ambient conditions, experimental K_S values span a range of 8%.

Our calculations fully confirm the strong influence of electronic thermal excitations.^{36,56} At the temperatures $T \sim 6000$ K of interest for the Earth's core, their contribution to the specific heat is almost as large as that due to lattice vibrations, in line with previous estimates. They also have a significant effect on the Grüneisen parameter γ , which plays a key role in the thermodynamics of the core, and is poorly constrained by experiment. Our finding that γ decreases with increasing pressure for $T < 4000$ K accords with an often-used rule of thumb,⁵⁸ but electronic excitations completely change this behavior at core temperatures $T \sim 6000$ K, where γ has almost constant values of ca. 1.45, in accord with experimental estimates in the range 1.1 to 1.6.^{21,63} Comparison with the earlier tight-binding calculations of Wasserman *et al.*³⁶ both for γ and for the quantity αK_T is not fully satisfactory. We find two kinds of disagreement at low temperatures. First, they find an increase of αK_T as $p \rightarrow 0$, whereas we find the opposite. Even more seriously, their strong increase of γ as $p \rightarrow 0$ is completely absent in our results. The source of these disagreements requires further investigation.

In summary, we have presented extensive *ab initio* calculations of the free energy and a range of other thermodynamic properties of iron at high pressures and temperatures, in which all statistical-mechanical errors are fully under control, and a high (and quantified) precision has been achieved. We find close agreement with the most reliable shock data. *Ab initio* values are provided for important, but experimentally poorly determined quantities, such as the Grüneisen parameter.

ACKNOWLEDGMENTS

The work of D.A. is supported by NERC Grant GST/02/1454 to G. D. Price and M. J. Gillan and by the Royal Society. We thank NERC and EPSRC for allocations of time on the Cray T3E machines at Edinburgh Parallel Computer Center and Manchester CSAR service, these allocations be-

ing provided through the Minerals Physics Consortium (GST/02/1002) and the UK Car-Parrinello Consortium (GR/M01753). We gratefully acknowledge discussions with Professor J.-P. Poirier and Dr. L. Vócadlo, and helpful comments on the original version of the manuscript by Professor R. E. Cohen.

APPENDIX REFERENCE MODELS FOR ANHARMONIC FREE ENERGY

Our calculation of the anharmonic part F_{anharm} of the *ab initio* free energy makes use of a reference system whose total energy is a linear combination of the *ab initio* harmonic energy and the energy of a model based on a purely repulsive pair potential (see Sec. II D 3). We have shown that this reference system gives an efficient way of computing F_{anharm} . However, we recognize that our choice of reference system may seem surprising, since it is well known that models based only on pair potentials cannot give a complete account of the energetics of transition metals. The known inadequacies of such models led many years ago to improved schemes such as the embedded-atom model (EAM)^{64,65} and other closely related models.^{66,67} This appendix has several aims: first, we clarify the sense in which our chosen reference system gives a computational scheme that is not only correct but also efficient; second, we recall the ways in which pair-potential descriptions of transition metals are inadequate, but we note that these ways are not necessarily relevant to the calculation of anharmonic free energies; third, we present numerical results that allow us to study how the calculation of F_{anharm} works if the EAM is used as the reference model for the anharmonic free energy, and we conclude that little is gained by doing this; finally, we explain the latter conclusion by showing that the EAM reduces almost exactly to a repulsive pair-potential model for the present anharmonic calculations. A more general analysis of the ideas that follow will be reported elsewhere.

We start by emphasizing that the final results for F_{anharm} cannot depend on the choice of reference model. This is simply because the free energy is a function of state, and the reversible work performed in going from the harmonic to the anharmonic system cannot depend on the path followed. But the path is specified by the choice of reference model. It follows that this choice cannot affect the numerical value of F_{anharm} . The choice of reference model is nevertheless crucial, because it determines the computational effort needed to obtain F_{anharm} . There are three separate reasons for this. The first reason is that thermodynamic integration requires the evaluation of $\langle U_1 - U_0 \rangle_\lambda$ [see Eq. (14)], where in the present case U_0 is the reference system and U_1 is the full *ab initio* system. Since $\langle U_1 - U_0 \rangle_\lambda$ can only be evaluated by statistical sampling and involves costly *ab initio* calculations, it is important to minimize the amount of sampling, i.e., the length of the simulation run needed to bring the statistical uncertainty below the specified tolerance on the precision (recall that the target tolerance in the present work is 10 meV/atom). But this uncertainty is governed by the fluctuation of the quantity $U_1 - U_0$ being averaged, so the criterion for a ‘‘good’’ U_0 is that the strength of the fluctuations of the

difference $\Delta U = U_1 - U_0$ between *ab initio* and reference total energies, i.e., the quantity $\langle \delta \Delta U^2 \rangle_\lambda$, be minimal, where $\delta \Delta U = \Delta U - \langle \Delta U \rangle_\lambda$.

The second reason for choosing U_0 carefully is that we want to reduce the number of λ points needed to perform the integration over λ . But this number is determined by the variation of the average $\langle U_1 - U_0 \rangle_\lambda$ as λ goes from 0 to 1. It is readily shown that if U_0 is close to U_1 then this variation is also completely determined by the fluctuation strength $\langle \delta \Delta U^2 \rangle_\lambda$, so one arrives at the same criterion as before for choosing U_0 . The third reason is that one wishes to suppress system-size errors. Since the evaluation of the free energy F_0 associated with U_0 is extremely rapid, it can be performed for very large systems, and size errors can be eliminated in F_0 . All the errors are therefore concentrated in $F_1 - F_0$, and hence in $\langle U_1 - U_0 \rangle_\lambda$. By minimizing the fluctuation strength, one also helps to make $\langle U_1 - U_0 \rangle_\lambda$ as small as possible, so that size errors have the least possible influence.

For all these three reasons, the key criterion in the choice of reference system is that the fluctuation strength be minimal; provided one is concerned only with computational efficiency and the correct calculation of F_{anharm} to a specified precision, then nothing else matters.

In the light of this criterion, we now ask whether the choice of a reference system based on pair potentials rather than on some more sophisticated model like EAM makes our task more difficult. The main problem with using pair potentials for metals is that they give a fundamentally wrong description of the changes of electronic bonding associated with changes of coordination. A real-space analysis shows⁶⁸ that the bonding energy of an atom in a metal should be roughly proportional to $z^{1/2}$, with z its coordination number, whereas a pair potential model will give an erroneous proportionality to z . The consequence is that the formation energies of coordination defects such as vacancies or surfaces will be wrongly given by a pair model. However, in calculating the anharmonic free energy, no significant changes of coordination are involved, so that the reference model is not being asked to do anything where a pair model would show its inadequacy. All the reference model has to do is to describe correctly the energy fluctuations of the anharmonically vibrating crystal, i.e., to give a small value of the fluctuation strength $\langle \delta \Delta U^2 \rangle_\lambda$, and the fact that it cannot describe surfaces or vacancies is irrelevant. (The concentration of real vacancies in a high temperature crystal might or might not be negligible, but this is not the point at issue here. In fact, for reasons discussed elsewhere,³ the effect of vacancies on the free energy of the real crystal is almost certainly negligible.)

The practical effectiveness of a reference system based on a combination of harmonic *ab initio* and a pair-potential model was demonstrated in Secs. V A and V B. Given the very small size of the fluctuation strength quoted there, our specified tolerance of 10 meV is already obtained with very little statistical sampling and with a single λ point, and size errors also fall within the tolerance. Nevertheless, the recent use of the EAM by other research groups^{44,45} to study high-*p*/high-*T* Fe makes it interesting to consider the consequences of using the EAM as a reference system in the present work.

To study this, we have made trial calculations based on the EAM recently used by Belonoshko *et al.*⁴⁵ to calculate the high-pressure melting curve of Fe. This EAM has the standard form⁶⁵ in which the total energy $E_{\text{tot}} = \sum_i E_i$ is a sum of energies E_i of atoms i , and each E_i consists of two parts: first, a purely repulsive energy E_i^{rep} represented as a sum of inverse-power pair potentials $E_i^{\text{rep}} = \sum_j' \epsilon (a/r_{ij})^n$, where r_{ij} is the interatomic separation and the sum excludes $i=j$; second, an “embedding” part $F(\rho_i)$ which accounts for the metallic bonding mainly due to partial filling of the d -bands. The embedding function $F(\rho)$ is represented as $-\epsilon C \rho^{1/2}$, and the density ρ_i for atom i is given by the sum over neighbors $\rho_i = \sum_j' (a/r_{ij})^m$. The parameters in this EAM were determined in Ref. 45 by fitting to first-principles energies of hcp and liquid Fe calculated using the full-potential linearized muffin-tin orbital (FPLMTO) technique. To check the quality of this EAM as a reference model, we have studied the energies it produces for a thermal sample of configurations generated by direct molecular dynamics simulation of a 64-atom cell of hcp Fe performed using our PAW technique at the state $T=6700$ K and $V=7.186$ Å³/atom, which is close to our preliminary calculated melting curve.⁴³ We find that the EAM and PAW energies are fairly close, but that the agreement can be further improved by adjusting the strength and exponent of the EAM inverse-power potential in E_i^{rep} , leaving the embedding energy $F(\rho_i)$ untouched. On doing this, we find the exponent $n=5.93$, which is very close to the value we obtained when we used the inverse power potential alone (see Sec. V A). The quality of fit of the EAM to our PAW energies can be characterized by the quantity $Q = [\langle \delta \Delta U^2 \rangle / N]^{1/2}$, where the fluctuation strength is calculated here as a time average in the m.d. run. We find the value $Q=0.09$ eV. If we do exactly the same thing using the pure inverse-power reference model described in the text, we also find the value $Q=0.09$ eV, so that the quality of the EAM as a reference model is not significantly different from that of the inverse-power model. We also note that the phonon frequencies obtained from the EAM are almost the same as those of the pure inverse-power reference system (see Sec. IV B).

We have used the EAM by itself as a reference model, without further changes of parameters, to calculate the anharmonic free energy of our PAW system at three thermodynamic states: $T=6000$ K, $V=6.97$ Å³/atom; $T=4500$ K, $V=8.67$ Å³/atom; and $T=4000$ K, $V=8.67$ Å³/atom. The calculations are done in three stages: first, we calculate the harmonic phonon frequencies of the EAM, and hence its harmonic free energy; next, we use thermodynamic integra-

tion to go from the harmonic EAM to the full EAM; finally, we use the second-order formula given in Eq. (17) to determine the difference between full EAM and PAW free energies. From this, we subtract the harmonic free energy F_{harm} of the PAW system to obtain the anharmonic free energy F_{anharm} . The resulting values of F_{anharm} at the three states mentioned above are -0.044 , -0.042 , and -0.039 eV, respectively, which should be compared with the values -0.057 , -0.048 , and -0.038 eV given by the fitting function discussed in the text (see Sec. V B). The agreement is satisfactory bearing in mind the statistical errors of typically 10 meV on all values. The important fact here is not that F_{anharm} comes out essentially the same as before, which is expected, but that the quality of the EAM as a reference system, though good, is no better than that of the reference model described in the text.

The conclusion from these numerical tests is that reference systems based either on the EAM or on purely repulsive pair potentials can be made to reproduce almost perfectly the *ab initio* total energy of the high- T anharmonic Fe system. But clearly this implies that these two types of reference system must be almost identical to each other for the atomic configurations sampled in thermal equilibrium. This implication may at first be surprising, but becomes less so if one considers what the EAM does. All the metallic bonding in the EAM is in the embedding density ρ_i for each atom. Even at high T , we find that this fluctuates only weakly. Writing $\rho_i = \bar{\rho} + \delta\rho_i$, where $\bar{\rho}$ is the thermal average of ρ_i , we can then write $F(\rho_i) \approx F(\bar{\rho}) + F'(\bar{\rho})\delta\rho_i$. With this approximation, the EAM reduces to a pair-potential model, since $\delta\rho_i$ consists of a sum over atom pairs. The pair potential in this “reduced” form of the EAM consists of a strongly varying repulsive term E_i^{rep} and a weakly varying bonding term $F'(\bar{\rho})\delta\rho_i$. To quantify this, we have examined the numerical size of the fluctuations of these two terms. We find that the mean square values of E_i^{rep} fluctuations are typically between 30 and 50 times those of $F(\rho_i)$ fluctuations. Closer analysis shows that this large factor comes from three sources: first, the square-root dependence of $F(\rho)$ on ρ ; second, the lower inverse-power exponent in ρ_i compared with that in E_i^{rep} ; third, the fact that E_i^{rep} is numerically about twice $F(\rho_i)$ at the pressures of interest. Since the fluctuations of E_i^{rep} are so dominant, the crucial requirement in using the EAM as a reference model is that the repulsive potential be optimized: one loses little by ignoring the fluctuations of the embedding energy and treating the latter simply as a volume-dependent constant. In this sense, the EAM reduces almost exactly to our reference model based on pair potentials.

¹L. Stixrude, R. E. Cohen, and R. J. Hemley, *Rev. Mineral.* **37**, 639 (1998).

²O. Sugino and R. Car, *Phys. Rev. Lett.* **74**, 1823 (1995).

³G. A. de Wijs, G. Kresse, and M. J. Gillan, *Phys. Rev. B* **57**, 8223 (1998).

⁴D. Alfè, G. A. de Wijs, G. Kresse, and M. J. Gillan, *Int. J. Quan-*

tum Chem. **77**, 871 (2000).

⁵J.-P. Poirier, *Introduction to the Physics of the Earth's Interior* (Cambridge University Press, Cambridge, England, 1991).

⁶J.-P. Poirier, *Phys. Earth Planet. Inter.* **85**, 319 (1994).

⁷T. G. Masters and P. M. Shearer, *J. Geophys. Res.*, [*Space Phys.*] **95**, 21 691 (1990).

- ⁸L. Stixrude, E. Wasserman, and R. E. Cohen, *J. Geophys. Res.*, [Space Phys.] **102**, 24 729 (1997).
- ⁹H. K. Mao, Y. Wu, L. C. Chen, J. F. Shu, and A. P. Jephcoat, *J. Geophys. Res.*, [Space Phys.] **95**, 21 737 (1990).
- ¹⁰R. Boehler, N. von Barga, and A. Chopelas, *J. Geophys. Res.*, [Space Phys.] **95**, 731 (1990).
- ¹¹R. Boehler, *Nature (London)* **363**, 534 (1993).
- ¹²S. K. Saxena, G. Shen, and P. Lazor, *Science* **260**, 1312 (1993).
- ¹³S. K. Saxena, G. Shen, and P. Lazor, *Science* **264**, 405 (1994).
- ¹⁴S. K. Saxena, L. S. Dubrovinsky, P. Häggkvist, Y. Cerenius, G. Shen, and H. K. Mao, *Science* **269**, 1703 (1995).
- ¹⁵S. K. Saxena, L. S. Dubrovinsky, and P. Häggkvist, *Geophys. Res. Lett.* **23**, 2441 (1996).
- ¹⁶A. P. Jephcoat and S. P. Besedin, *Philos. Trans. R. Soc. London, Ser. A* **354**, 1333 (1996).
- ¹⁷D. Andraut, G. Fiquet, M. Kunz, F. Visocekas, and D. Häusermann, *Science* **278**, 831 (1997).
- ¹⁸G. Shen, H. Mao, R. J. Hemley, T. S. Duffy, and M. L. Rivers, *Geophys. Res. Lett.* **25**, 373 (1998).
- ¹⁹L. Vočadlo, J. Brodholt, D. Alfè, M. J. Gillan, and G. D. Price, *Phys. Earth Planet. Inter.* **117**, 123 (2000).
- ²⁰R. Jeanloz, *J. Geophys. Res.*, [Space Phys.] **84**, 6059 (1979).
- ²¹J. M. Brown and R. G. McQueen, *J. Geophys. Res.*, [Space Phys.] **91**, 7485 (1986).
- ²²C. S. Yoo, N. C. Holmes, M. Ross, D. J. Webb, and C. Pike, *Phys. Rev. Lett.* **70**, 3931 (1993).
- ²³M. Matsui and O. L. Anderson, *Phys. Earth Planet. Inter.* **103**, 55 (1997).
- ²⁴A. B. Belonoshko and R. Ahuja, *Phys. Earth Planet. Inter.* **102**, 171 (1997).
- ²⁵P. Hohenberg and W. Kohn, *Phys. Rev.* **136**, B864 (1964); W. Kohn and L. Sham, *Phys. Rev.* **140**, A1133 (1965); R. O. Jones and O. Gunnarsson, *Rev. Mod. Phys.* **61**, 689 (1989); M. J. Gillan, *Contemp. Phys.* **38**, 115 (1997).
- ²⁶C. S. Wang, B. M. Klein, and H. Krakauer, *Phys. Rev. Lett.* **54**, 1852 (1985).
- ²⁷L. Stixrude, R. E. Cohen, and D. J. Singh, *Phys. Rev. B* **50**, 6442 (1994).
- ²⁸P. Söderlind, J. A. Moriarty, and J. M. Willis, *Phys. Rev. B* **53**, 14 063 (1996).
- ²⁹L. Vočadlo, G. A. de Wijs, G. Kresse, M. J. Gillan, and G. D. Price, *Faraday Discuss.* **106**, 205 (1997).
- ³⁰H. K. Mao, J. Xu, V. V. Struzhkin, J. Shu, R. J. Hemley, W. Sturhahn, M. Y. Hu, E. E. Alp, L. Vočadlo, D. Alfè, G. D. Price, M. J. Gillan, M. Schwoerer-Böhning, D. Häusermann, P. Eng, G. Shen, H. Giefers, R. Lübbers, and G. Wortmann, *Science* **292**, 914 (2001).
- ³¹G. A. de Wijs, G. Kresse, L. Vočadlo, D. Dobson, D. Alfè, M. J. Gillan, and G. D. Price, *Nature (London)* **392**, 805 (1998).
- ³²D. Alfè, G. Kresse, and M. J. Gillan, *Phys. Rev. B* **61**, 132 (2000).
- ³³D. Alfè and M. J. Gillan, *Phys. Rev. B* **58**, 8248 (1998).
- ³⁴D. Alfè and M. J. Gillan, *Phys. Rev. Lett.* **81**, 5161 (1998).
- ³⁵D. Alfè, G. D. Price, and M. J. Gillan, *Phys. Earth Planet. Inter.* **110**, 191 (1999).
- ³⁶E. Wasserman, L. Stixrude, and R. E. Cohen, *Phys. Rev. B* **53**, 8296 (1996).
- ³⁷A. C. Holt and M. Ross, *Phys. Rev. B* **1**, 2700 (1970).
- ³⁸Y. Wang and J. P. Perdew, *Phys. Rev. B* **44**, 13 298 (1991).
- ³⁹J. P. Perdew, J. A. Chevary, S. H. Vosko, K. A. Jackson, M. R. Pederson, D. J. Singh, and C. Fiolhais, *Phys. Rev. B* **46**, 6671 (1992).
- ⁴⁰P. E. Blöchl, *Phys. Rev. B* **50**, 17 953 (1994).
- ⁴¹G. Kresse and D. Joubert, *Phys. Rev. B* **59**, 1758 (1999).
- ⁴²S. H. Wei and H. Krakauer, *Phys. Rev. Lett.* **55**, 1200 (1985).
- ⁴³D. Alfè, M. J. Gillan, and G. D. Price, *Nature (London)* **401**, 462 (1999).
- ⁴⁴A. Laio, S. Bernard, G. L. Chiarotti, S. Scandolo, and E. Tosatti, *Science* **287**, 1027 (2000).
- ⁴⁵A. B. Belonoshko, R. Ahuja, and B. Johansson, *Phys. Rev. Lett.* **84**, 3638 (2000).
- ⁴⁶D. Vanderbilt, *Phys. Rev. B* **41**, 7892 (1990).
- ⁴⁷N. D. Mermin, *Phys. Rev.* **137**, A1441 (1965).
- ⁴⁸M. J. Gillan, *J. Phys.: Condens. Matter* **1**, 689 (1989).
- ⁴⁹R. M. Wentzcovitch, J. L. Martins, and P. B. Allen, *Phys. Rev. B* **45**, 11 372 (1992).
- ⁵⁰G. Kresse and J. Furthmüller, *Phys. Rev. B* **54**, 11 169 (1996).
- ⁵¹G. Kresse and J. Furthmüller, *Comput. Mater. Sci.* **6**, 15 (1996).
- ⁵²H. J. Monkhorst and J. D. Pack, *Phys. Rev. B* **13**, 5188 (1976).
- ⁵³G. Kresse, J. Furthmüller, and J. Hafner, *Europhys. Lett.* **32**, 729 (1995).
- ⁵⁴D. Frenkel and B. Smit, *Understanding Molecular Simulation* (Academic, San Diego, 1996).
- ⁵⁵H. C. Andersen, *J. Chem. Phys.* **72**, 2384 (1980).
- ⁵⁶D. A. Boness and J. M. Brown, *J. Geophys. Res.*, [Space Phys.] **95**, 21 721 (1990); D. A. Boness, J. M. Brown, and A. K. McMahan, *Phys. Earth Planet. Inter.* **42**, 227 (1986).
- ⁵⁷N. W. Ashcroft and N. D. Mermin, *Solid State Physics* (Holt, Rinehart and Winston, New York, 1976), Chap. 2.
- ⁵⁸It is often assumed that the thermodynamic Grüneisen parameter γ is independent of temperature and depends on volume as $(V/V_0)^q$, where V_0 is a reference volume and q is a positive exponent roughly equal to unity; see, e.g., O. L. Anderson, *Equations of State of Solids for Geophysics and Ceramic Science*, Oxford Monographs on Geology and Geophysics No. 31 (Oxford University Press, New York, 1995).
- ⁵⁹S. H. Vosko, L. Wilk, and M. Nusair, *Can. J. Phys.* **58**, 1200 (1980).
- ⁶⁰See, e.g., Chap. 4 of Ref. 5.
- ⁶¹We obtain the C_v values from Refs. 8 and 36 by using the formula given in Eq. (10) of Ref. 8 for the electronic contribution and the Dulong-Petit value $3k_B$ /atom for the lattice contribution. The C_v values of Refs. 8 and 36 refer to the fcc phase of Fe.
- ⁶²T. S. Duffy and T. J. Ahrens, *Geophys. Res. Lett.* **20**, 1103 (1993).
- ⁶³F. Stacey, *Phys. Earth Planet. Inter.* **89**, 219 (1995).
- ⁶⁴M. S. Daw and M. I. Baskes, *Phys. Rev. B* **29**, 6443 (1984).
- ⁶⁵M. S. Daw, S. M. Foiles, and M. I. Baskes, *Mater. Sci. Rep.* **9**, 251 (1993).
- ⁶⁶M. W. Finnis and J. E. Sinclair, *Philos. Mag. A* **50**, 45 (1984).
- ⁶⁷K. W. Jacobsen, J. K. Norskov, and M. J. Puska, *Phys. Rev. B* **35**, 7423 (1987).
- ⁶⁸D. G. Pettifor, *Bonding and Structure of Molecules and Solids* (Clarendon, Oxford, 1995), pp. 131, 188.
- ⁶⁹A. Dal Corso and S. de Gironcoli, *Phys. Rev. B* **62**, 273 (2000).